

# Path integral Monte Carlo simulations of silicates

Chr. Rickwardt<sup>1,\*</sup>, P. Nielaba<sup>2</sup>, M. H. Müser<sup>1</sup>, K. Binder<sup>1</sup>

<sup>1</sup> *Institut für Physik, Johannes Gutenberg Universität Mainz, 55099 Mainz, Germany*

<sup>2</sup> *Fachbereich Physik, Universität Konstanz, Fach M 691, 78457 Konstanz, Germany*

(November 10, 2018)

## Abstract

We investigate the thermal expansion of crystalline  $\text{SiO}_2$  in the  $\beta$ -cristobalite and the  $\beta$ -quartz structure with path integral Monte Carlo (PIMC) techniques. This simulation method allows to treat low-temperature quantum effects properly. At temperatures below the Debye temperature, thermal properties obtained with PIMC agree better with experimental results than those obtained with classical Monte Carlo methods.

## I. INTRODUCTION

The study and analysis of materials properties of crystalline silicates are important since these systems are used in many industrial processes and they occur also in many natural rocks. Many interesting effects have been found by experimental techniques at temperatures well below the Debye temperature. In this temperature range quantum effects like zero point motions and corresponding delocalizations of atoms are important which have to be taken into account in serious theoretical studies. Usually this is done by lattice dynamics theories, in the framework of the harmonic or quasiharmonic approximation. However, both near second-order structural phase transitions and quite generally at higher temperatures the

---

\*present address: Landesbank Rheinland-Pfalz, Mainz, Germany

accuracy of this approach is sometimes uncertain<sup>1</sup>, and methods that work at all conditions would be desirable.

PIMC simulations<sup>2</sup> enable us to analyse the crystal low temperature thermal properties. In principle, this method yields exact quantum-statistical averages (apart from statistical errors) and reduces to classical statistical averages at high temperatures. In general the agreement with experimental data is better compared to classical computations. For  $\beta$ -cristobalite it turns out that even at temperatures as high as 600 K only with PIMC a good agreement with experimental findings is obtained. The negative thermal expansion in  $\beta$ -quartz however may be explained by a classical modelling.

The outline of this paper now is as follows: in Sec. II we define the models that are studied, in Sec. III we briefly review the PIMC technique, while Sec. IV describes our results in detail. We conclude in Sec. V with a brief summary.

## II. THE MODEL

Starting from the diamond lattice of silicon solids and placing between each neighbour pair of Si atoms an O atom, we arrive at a silicate which exists in nature in cubic symmetry:  $\beta$ -cristobalite.

For the computation of  $\text{SiO}_2$ -structures a variety of potentials are studied in the literature, for a review see ref.<sup>3</sup>. Concerning the computational time it is of great advantage that apparently two-body potentials like the TTAM-potential<sup>4</sup> and the BKS-potential<sup>5</sup> describe the system properties at least as good as three body potentials. Thus most of the investigations presented here have been done with the TTAM- and the BKS- potentials. Comparative studies have been done as well with other potentials like the two-body contribution of a complicated potential obtained via ab-initio computations<sup>6</sup> (“core-shell”-potential).

In case of the TTAM and the BKS potentials the interactions between the Si and O-ions are modelled by pair potentials of the form:

$$\Phi(r_{ij}) = \frac{Q_i Q_j e^2}{r_{ij}} + A_{ij} \exp(-B_{ij} r_{ij}) - \frac{C_{ij}}{r_{ij}^6} \quad (1)$$

Here  $e^2 = \frac{1602.19}{4.8.8542 \cdot \pi} eV \text{\AA}$ . In Eq.(1) each ion carries a partial charge: A Si- ion has the charge  $Q = 2.4$  and an O- ion has the charge  $Q = -1.2$ .

The TTAM potential has been developed by Tsuneyuki et.al.<sup>4</sup>. The parameters in Eq.(1) are listed in table I. The parameters in Eq.(1) for the BKS- potential<sup>5</sup> are tabulated in table II.

In general complex materials with several components interacting with long ranged Coulomb interactions have to be handled by appropriate numerical procedures such as the Ewald summation technique. In the numerical simulation the computation of the Coulomb contribution to the energy requires a summation not only over the particle indices but also over all periodic boxes:

$$E_{coul} = \frac{1}{2} \sum_{\vec{n}} \sum_{\substack{i,j \\ (i \neq j \text{ for } \vec{n} = \vec{0})}} \frac{Q_i Q_j e^2}{|\vec{r}_{ij} + \vec{n}|} \quad (2)$$

The sum in Eq.(2) is over all periodic images shifted by  $\vec{n}$  and all particle indices except  $i = j$  for  $\vec{n} = \vec{0}$ . For numerical details of the computation of the Coulomb energy and how to use a relatively simple and efficient algorithm we refer to Ref.<sup>7</sup>

Both potentials have in common that at small interparticle distances the atomic repulsion is neglected and rather a divergency in the potentials at small distances appears. In order to avoid a ‘‘Coulomb-collapse’’ of the system, at small distances we have to include an additional repulsive term. This term can be modelled as a harmonic contribution<sup>8</sup> suitable for molecular dynamics simulations or as a purely hard sphere repulsion. In this study for the sake of simplicity we follow the latter prescription, the hard sphere distance is chosen as the distance of the first potential maximum in Eq. (1).

### III. PATH INTEGRAL MONTE CARLO SIMULATIONS

Canonical averages  $\langle A \rangle$  of an observable  $A$  in a system defined by the Hamiltonian  $\mathcal{H} = E_{kin} + V_{pot}$  of  $N$  particles in a volume  $V$  are given by:

$$\langle A \rangle = Z^{-1} \text{Sp} [A \exp(-\beta \mathcal{H})] \quad . \quad (3)$$

Here  $Z = \text{Sp} [\exp(-\beta \mathcal{H})]$  is the partition function and  $\beta = 1/k_B T$  is the inverse temperature. Utilising the Trotter-product formula,

$$\exp(\beta \mathcal{H}) = \lim_{P \rightarrow \infty} (\exp(-\beta E_{kin}/P) \exp(-\beta V_{pot}/P))^P \quad , \quad (4)$$

we obtain the path integral expression<sup>2</sup> for the partition function:

$$Z(N, V, T) = \lim_{P \rightarrow \infty} \left( \frac{mP}{2\pi\beta\hbar^2} \right)^{3NP/2} \prod_{s=1}^P \int d\{\mathbf{r}^{(s)}\} \exp\left[-\frac{\beta}{P} \left( \sum_{k=1}^N \frac{mP^2}{2\hbar^2\beta^2} (\mathbf{r}_k^{(s)} - \mathbf{r}_k^{(s+1)})^2 + V_{pot}(\{\mathbf{r}^{(s)}\}) \right)\right] \quad (5)$$

Here,  $m$  is the particle mass, integer  $P$  is the Trotter number and  $\mathbf{r}_k^{(s)}$  denotes the coordinate of particle  $k$  at Trotter-index  $s$ , and periodic boundary conditions apply, the particle with Trotter-index  $P + 1$  is the same as the particle with Trotter-index 1. This formulation of the partition function allows us to perform Monte Carlo simulations for increasing values of  $P$  approaching the true quantum limit for  $P \rightarrow \infty$ . Note that Eq. (5) does not take into account any quantum-mechanical exchange between particles (for atoms as heavy as Si and O this is an excellent approximation, though it would not work for He crystals).

Thermal averages in the ensemble with constant pressure  $p$  are given via the corresponding partition function

$$\Delta(N, p, T) = \int_0^\infty dV \exp[-\beta pV] Z(N, V, T) \quad (6)$$

. In order to make our results comparable with those of experiments, our PIMC simulations have been performed in the constant pressure ensemble. Most of our simulations<sup>9</sup> have been done with  $N = 684$  particles ( $\beta$ -cristobalite),  $N = 576$  ( $\beta$ -quartz),  $p = 0$ , and  $P$ -values up to 100. A typical PIMC data point in figure 2 required about 1200 CPU hours on a CRAY-T3E (single processor).

#### IV. RESULTS

### A. Finite size effects and pair potential sensitivity

In order to analyse effects due to the finite system size simulations for the system in the  $\beta$ -cristobalite structure have been done using the three potentials described above and  $N = 648$  particles as well as with the BKS- potential and  $N = 192$  particles. In Figs. 1 and 2 the potential energy and the systems box volume is shown.

The energy obtained by the core-shell potential (in the two-body reduced form) is significantly smaller than the energy obtained by the other two potentials. The volume obtained by the core-shell potential is much larger than the experimental data<sup>10</sup> and the thermal expansion coefficient is negative over the entire temperature range studied- in contrast to the experimental results for  $\beta$ -cristobalite.

For the BKS- potentials the successful description of SiO<sub>2</sub>-melt properties<sup>8</sup> using a cut-off distance of 5.5Å for the short ranged interactions suggested the choice of this cutoff-distance in the present study as well. From figure 1 however it is apparent that the volume decreases strongly with increasing temperature- in contrast to the experimental data. For the ordered crystal it turned out that a larger cutoff value (12 Å) is more adequate for the description of the system properties.

The energies obtained by the TTAM- potential and by the BKS- potential (for both system sizes) agree well. In case of the volume however the results for the BKS- potential agree for both system sizes within numerical scatter and show a qualitatively similar temperature dependence as the volume obtained by the TTAM- potential. The quantitative values of the volume for the TTAM- potential however are much larger than the experimental data, whereas the volume obtained by the BKS- potential agrees well with the experimental data for temperatures above 700 K.

In summary the best agreement with the experimental data can be obtained with the BKS- potential - at least in a temperature range above 700 K. For smaller temperatures apparently none of the classical computations can successfully describe the experimental data.

## B. Quantum simulations for $\beta$ - cristobalite

### 1. Potential energy and volume

A different picture emerges if results of quantum simulations are considered in addition (BKS- potential,  $N = 648$ ), see figure 2. At temperatures below 700 K the quantum results for the potential energies deviate from the classical results to higher values, but for higher temperatures they agree with the classical values. The volume of the simulation box obtained by the PIMC simulations (Fig. 2) agree within numerical scatter with the experimental data for all temperatures studied- in contrast to the classical simulations. Despite the apparently high temperatures of 700 K quantum effects are very important for the thermal properties of  $\beta$ -cristobalite and thus quantum effects should not be neglected in simulations of real materials. This supports the assumption that quantum effects may still play an important role above the Debye temperature which is at about 500 K for  $\text{SiO}_2$ .

### 2. Structural details

According to a model of Wyckoff<sup>11,12</sup> for  $\beta$ - cristobalite the O- atoms are located in the middle of a bond connecting two Si- atoms, the Si–O–Si bond angle is  $180^\circ$  and the Si-O bond length  $1.54 \text{ \AA}$ . In order to correct these values to obtain the actually observed angle (between  $140^\circ$  and  $150^\circ$ ) and bond lengths (Si-O: about  $1.61 \text{ \AA}$ ) several models have been suggested in which the O- positions deviate from the ideal middle places<sup>13–17</sup>. The question which of these models describes the properties of  $\beta$ - cristobalite best is not yet decided by experimental methods.

In figure 3 we show the bond length distribution function for the different atom pairs for three temperatures using the BKS potential and in figure 4 the average bond lengths as a function of temperature. Note that due to the choice of a finite size cubic simulation box with periodic boundary conditions,  $\beta$ -cristobalite is stable (or metastable, respectively) in the simulation over the entire temperature range, unlike experiment.

In the PIMC simulations (with  $P=30$ ) the bond lengths have larger values at low temperatures compared to the classical case ( $P=1$ ) (Fig. 4). The quantum results for the Si-O bond length are in much closer agreement with the literature value of  $1.61 \text{ \AA}$ . The Si-O as well as the O-O bond lengths scale approximately linearly with the temperature, the Si-Si bond length decrease is stronger in parallel to the temperature dependence of the volume. This may be due to the fact that the positions of the Si-atoms fix the lattice constant of  $\beta$ -cristobalite and the O- atoms have a much larger mobility in the crystal lattice. In figure 4 we find again the different behaviour of the Si-Si bonds compared to the other bonds. The temperature dependence of the Si-O and the O-O bonds have the following features:

- The width of the distributions increases with temperature, the height decreases.
- The average values increase with the temperature.
- At the same temperature the distributions obtained by PIMC ( $P=30$ ) have larger average values than the classical distributions.
- The difference in the distributions and the average values between the classical and the quantum results decrease with the temperature.

All these effects are present in the Si-Si bonds as well, but there is a significant difference: In Figs. 3 and 4 we find that for the other two bond types the differences between the classical and the quantum values at the temperature  $T$  are always smaller than the difference between the classical values at  $T$  and the next higher temperature studied. For the Si-Si bond the quantum distributions at 400 K are closer to the distributions at 1600 K (which do not differ very much any more) than to the classical distributions at 400 K. This shows that in particular the Si-Si bond properties are significantly determined by quantum effects.

In order to obtain more information on the long-range molecular structure, the radial distribution functions  $g(r)$  were computed up to a distance of  $10 \text{ \AA}$  for Si-Si, Si-O, and O-O bonds. The knowledge of  $g(r)$  allows the calculation of the so-called total correlation function  $T(r)$ , which is a superposition of the various  $g(r)$ 's.<sup>18</sup>  $T(r)$  has been measured

recently by neutron diffraction.<sup>18</sup> The measurements allowed to accurately estimate the real Si-O bond lengths and it was concluded that the typical Si-O bond length is considerably longer than the Si-O bond length in the so-called ideal  $\beta$ -cristobalite geometry. In Fig. (5a), a comparison between the experimentally observed and the calculated function  $T(r)$  is shown. The agreement between the two curves is at least semi quantitative and the conclusions drawn in Ref.<sup>18</sup> could be confirmed with the exception of the width of the first Si-O peak and the first O-O peak. These peaks are broadened in experiment with respect to simulations, which include quantum effects. The broadenings might be due to lattice defects or to internal surfaces in the experimental samples. Both kind of defects were absent in our simulations. Similar results on  $T(r)$  were reported previously by purely classical simulations<sup>19</sup> on the basis of the TTAM potential.

Fig. (5b) allows to relate the features in  $T(r)$  to the various  $g(r)$ 's. It is interesting to note that the peak in  $T(r)$  at about 5 Å is due to a simultaneous maximum in  $g_{\text{OO}}(r)$  and  $g_{\text{SiO}}(r)$ , while the peak in  $T(r)$  at 6.25 Å does not have a corresponding peak in any  $g(r)$ . The large local maximum in  $T(r)$  at about 9 Å is then located at a position where all  $g(r)$ 's have a local maximum as well. The shape of  $T(r)$  is particularly sensitive to details of the potentials at large distances, e.g., cutting off the short-range part of the potential at 4.5 Å alters  $T(r)$  significantly for  $r \geq 8$  Å.

### C. Quantum simulations for $\beta$ -quartz

The  $\beta$ - quartz structure differs from the  $\beta$ - cristobalite structure by the positions of the atoms in the unit cell.  $\beta$ - cristobalite has a cubic structure,  $\beta$ - quartz has a hexagonal structure and at a temperatures below 846 K a trigonal  $\alpha$ - quartz is stable<sup>21,22,20,23-25</sup>. For structural details of the  $\beta$ - quartz see appendix A. The piezoelectricity (and pyroelectricity) of  $\beta$ -quartz is at least reduced for  $\beta$ - cristobalite due to symmetry reasons.

As for  $\beta$ - cristobalite the simulations have been done for Trotter values of  $P=1$  and  $P=30$  at temperatures between 600 K and 1600 K. Generalizing Eqs. (3),(5) and (6), in our



constant pressure simulations a hydrostatic pressure  $p$  has been applied and fluctuation trials of the box lengths in  $x$ -,  $y$ - and  $z$ - directions have been attempted independently keeping the angles between the box axes constant. Lattice constants ( $a$  and  $c$ ) have been obtained from the resulting average box geometry. The experimentally observed transition at 846 K is suppressed in the simulations since we keep our box in rectangular shape. A trigonal  $\alpha$ - quartz structure thus cannot be stabilised, rather a metastable, undercooled  $\beta$ -quartz is present in the simulations. Above the phase transition temperature, the structure in the simulation agrees with the structure deduced from the experimental data.

In figure 6 the potential energy and lattice constants of  $\beta$ -quartz are compared to experimental data<sup>25</sup>. The energy has a linear temperature dependence in the classical case and slightly higher values in the quantum simulations, the difference to the classical values increases the lower the temperature. Apparently in this temperature region quantum effects become important- as can be expected due to a Debye- temperature of 500 K for SiO<sub>2</sub>. The temperature dependence of the volume only qualitatively agrees with the experimental data. In figure 6 we note the qualitatively different behaviour between the experiments and the simulation data at temperatures close to the  $\alpha \leftrightarrow \beta$  transition at 846 K. As explained above this different behaviour is caused by the box shape constraint in the simulation.

As in the experiment the lattice constant in  $a$ - direction is approximately temperature independent at high temperatures whereas in  $c$ - direction a negative thermal expansion coefficient is found. In the case of the lattice constant  $c$ , the PIMC results are in somewhat better agreement with the experimental data than the classical results. Since for  $\beta$ -cristobalite it turned out that by using the literature value (5.5 Å) for the cutoff the agreement with the experimental data is not as good as without the cutoff (see above), we chose the maximum cutoff value which is possible in our box geometry. The deviation of 1% ( $c$ -direction) and 0.3% ( $a$ - direction) from the experimental values may be due to the choice of parameters in the interaction potential, in particular to the cutoff of the short ranged interactions in the BKS- potential. Probably a restriction to smaller cutoff values would result in a better agreement with experimental data.

A typical simulation data point in figure 6 also required a computational effort of about 1200 CPU hours on a CRAY-T3E computer (in units of single-processor time).

Surprisingly the *c*- lattice constant obtained by a classical simulation decreases slightly with increasing temperature. This behaviour- which is present in the experimental data as well- may thus be explained by a purely classical argument. In the literature the ‘rigid unit modes’<sup>26–28</sup> are suggested as being responsible for the negative thermal expansion coefficient. For the sake of a more complete discussion of our results, we recall this argument here: The idea is that in a covalently bonded crystal structure one can identify units which are essentially rigid, because the length of the covalent bonds are essentially rigid, but that at certain atomic positions where the rigid units are linked together, they may rotate relative to each other. These modes may be visualised schematically as in figure 7 for two dimensional structures. The quadratic bases in this example may correspond to SiO<sub>4</sub> tetrahedron in  $\beta$ - quartz. If the angle stabilising forces in such units are significantly stronger than the forces at the common O- atoms connecting such tetrahedron, thermal excitation leads to a rotation of the complete bases. In contrast to the positive thermal expansion coefficient caused by the anharmonicities of the interatomic interactions such collective modes may cause a negative thermal expansion coefficient. The possible mechanism is briefly sketched: By tilting of the unit cell by the angle  $\Theta$  the system volume  $A = A_0$  (see Fig. 7) changes to  $A = A_0 \cos^2(\Theta)$ . For small angles and harmonic rotational oscillations with frequency  $\omega$  of the units (i.e. tetrahedra) with moment of inertia  $I$  the resulting thermal average of  $A$  is<sup>26–28</sup>:

$$A(T) = \langle A \rangle_T = A_0(1 - \langle \Theta^2 \rangle_T) = A_0\left(1 - \frac{k_B T}{I\omega^2}\right) \quad (7)$$

The thermal average of the tilt angle  $\langle \Theta^2 \rangle_T$  increases with temperature and thus leads to a decrease of system volume. At low temperatures this effect may more than compensate the ‘normal’ thermal expansion caused by the motion of single atoms such that the thermal expansion coefficient is negative.

### 1. Structural details $\beta$ -quartz

In order to get more information on the molecular structure, the radial distribution functions  $g(r)$  were computed for  $\beta$ -quartz, again up to a distance of  $10 \text{ \AA}$ . The correlation function  $T(r)$ , which follows from the various  $g(r)$ 's, is shown in Fig. (8a) together with  $g_{\text{SiSi}}$ ,  $g_{\text{SiO}}$ , and  $g_{\text{OO}}$  in Fig. (8b).

It is instructive to compare Fig. (8) for  $\beta$ -quartz with the corresponding figure for  $\beta$ -cristobalite, Fig. (5). The location of the peaks in  $g(r)$  are nearly identical for nearest neighbor Si-Si, Si-O, and O-O peaks, only the peaks are broadened in the case of  $\beta$ -quartz, which can entirely be attributed to the larger temperature of the  $\beta$ -quartz simulation. It can be concluded that the tetrahedra formed by  $\text{SiO}_4$  units are basically identical for both lattice structures. While the radial distribution functions differ markedly between the two lattices for distances  $r > 3.5 \text{ \AA}$ , there is a much less pronounced, yet noticeable, effect in  $T(r)$ . E.g.,  $T(r)$  shows a shoulder for  $\beta$ -quartz at  $r \approx 3.7 \text{ \AA}$  which is absent in the simulation of  $\beta$ -cristobalite.

### D. “Size” of the quantum particles

By determining the average radius of the quantum-particles across the quantum chain their “size” can be mapped as a function of temperature. In figure 9 we compare the simulation results for these radii in the various lattice structures with the thermal de-Broglie wave lengths for free O- and Si- atoms. Apparently this quantity does not depend much on the particular lattice structure. This may be due to the fact that the quantum chain radius is determined by the close surrounding of the particles and the potentials. In both crystalline structures studied here the basic unit is a  $\text{SiO}_4$  tetrahedron and the BKS potential is used. The de-Broglie wave lengths for the free particles are much larger than the radii of the particles of the crystals. This may be due to the stronger binding and localisation of the latter.

## V. SUMMARY

In this paper we present the results of our PIMC simulations for crystalline silicates. With PIMC simulations we are able to analyse the thermal properties of crystals at temperatures at which quantum effects have to be considered as well as anharmonic effects. In general the agreement with experimental data is better compared to classical computations. For  $\beta$ -cristobalite it turns out that even at temperatures as high as 600 K only with PIMC a good agreement with experimental findings is obtained. The negative thermal expansion in  $\beta$ -quartz however may be explained by classical effects.

We conclude that for a realistic materials modelling the simulation by path integral Monte Carlo techniques is a useful method which should be used in future studies of thermal properties of other crystals as well.

## ACKNOWLEDGMENTS

C.R. thanks the SCHOTT- Glaswerke for support and P.N. thanks the DFG for support (Heisenberg foundation and SFB 513). The computations were carried out on the *CRAY T3E* of the *HLRZ* at Jülich.

## VI. APPENDIX A

In most simulations a rectangular simulation box is used. It is thus of advantage to map the hexagonal system onto a larger rectangular box such that the periodic order results in the hexagonal structure.<sup>9</sup>

The lattice structure for  $\beta$ - quartz is sketched in Fig. 10 and may be described as follows. In the space group  $P6_222$  the unit vectors are:

$$\begin{aligned}
\vec{e}_1 &= (4.9977, 0, 0) \\
\vec{e}_2 &= (-2.49885, 4.328135, 0) \\
\vec{e}_3 &= (0, 0, 5.4601)
\end{aligned}
\tag{8}$$

Thus the lattice constants are:

$$\begin{aligned}
a &= 4.9977\text{\AA} \\
b &= \sqrt{3}a \\
c &= 5.4601\text{\AA}
\end{aligned}
\tag{9}$$

The coordinates of the particles in a unit cell are given in table III, the Cartesian coordinates in table IV.

Due to the differences in box lengths one has to reduce the effect of different surface areas on the simulation results. This is done by matching sufficiently many unit cells such that the simulation box is approximately cubic.

## REFERENCES

- <sup>1</sup> G.C Rutledge, D.J. Lacks, R. Martonak, K. Binder; J. Chem. Phys. **108**, 10274 (1998).
- <sup>2</sup> R.P. Feynman and A.R. Hibbs, *Quantum Mechanics and Path Integrals* (McGraw–Hill, New York, 1965); H.F. Trotter, Proc. Am. Math. Soc. **10**, 545 (1959); Commun. Math. Phys. **51**, 183 (1976); J.A. Barker, J. Chem. Phys. **70**, 2914 (1979); K. S. Schweizer, R. M. Stratt, D. Chandler, P. G. Wolynes, J. Chem. Phys. **75**, 1347 (1981); D. M. Ceperley, Rev. Mod. Phys. **67**, 279 (1995); P. Nielaba, in *Annual Reviews of Computational Physics V* edited by D. Stauffer (World Scientific, Singapore), pp. 137 (1997).
- <sup>3</sup> K. Vollmayr, Ph.D thesis, Mainz (1995).
- <sup>4</sup> S. Tsuneyuki, M. Tsukada, H. Aoki, Y. Matsui; Phys. Rev. Lett. **61**, 869 (1988).
- <sup>5</sup> B. van Beest, G. Kramer, R. van Santen; Phys. Rev. Lett. **64**, 1955 (1990).
- <sup>6</sup> K.-P. Schröder, J. Sauer; J. Phys. Chem. **100**, 11043 (1996).
- <sup>7</sup> D. Frenkel and B. Smit, *Understanding Molecular Simulation: From Algorithms to Applications*, (Academic Press, San Diego, 1996).
- <sup>8</sup> K. Vollmayr, W. Kob, K. Binder; Phys. Rev. **B 54**, 15808 (1996).
- <sup>9</sup> Chr. Rickwardt, Ph.D thesis, Mainz (1998).
- <sup>10</sup> I.P. Swainson, M.T. Dove, Phys. Chem. Minerals **22**, 61 (1995).
- <sup>11</sup> R. Wyckoff; Am. J. Sci **9**, 448 (1925).
- <sup>12</sup> R. Wyckoff; Z. f. Krist. **62**, 189 (1925).
- <sup>13</sup> A. Wright, A. Leadbetter; Phil. Mag. **31**, 1391 (1975).
- <sup>14</sup> D. Hatch, S. Ghose; Phys. Chem. Min. **17**, 554 (1991).
- <sup>15</sup> M. Dove, A. Giddy, V. Heine; Ferroelectrics **136**, 33 (1992).

- <sup>16</sup> M. Dove, A. Giddy, V. Heine; *Trans. Am. Cryst. Assoc.* **27**, 697 (1992).
- <sup>17</sup> A. Giddy, M. Dove, G. Pawley, V. Heine; *Acta Cryst.* **A 49**, 697 (1993).
- <sup>18</sup> M. T. Dove, D. A. Kreen, A. C. Hannon, and I. P. Swainson, *Phys. Chem. Minerals* **24**, 311 (1997).
- <sup>19</sup> I. P. Swainson and M. T. Dove, *J. Phys. Cond.Matt.* **7** 1771 (1995).
- <sup>20</sup> J. Tse, and D. Klug; *Phys. Rev. Lett.* **67**, 3559 (1991); *Science* **255**, 1559 (1992).
- <sup>21</sup> J. Tse, D. Klug, Y. LePage; *Phys. Rev. Lett.* **69**, 3647 (1992).
- <sup>22</sup> J. Tse, D. Klug, Y. LePage; *Phys. Rev.* **B 46**, 5933 (1992).
- <sup>23</sup> F. Liu, S. H. Garofalini, R. D. King–Smith, D. Vanderbilt; *Phys. Rev. Lett.* **70**, 2750 (1993).
- <sup>24</sup> J. Axe, G. Shirane; *Phys. Rev.* **B 1**, 342 (1970).
- <sup>25</sup> K. Kihara; *Eur. J. Mineral.* **2**, 63 (1990).
- <sup>26</sup> P. Welche, V. Heine, M. Dove; *Phys. and Chem. of Minerals*. Berlin: Springer (1997).
- <sup>27</sup> M. Dove, V. Heine, K. Hammonds; *Mineral. Mag* **59**, 629 (1997).
- <sup>28</sup> M. Gambhir, M.T. Dove, V. Heine; *Phys. Chem. Minerals* **26**, 484 (1999).

FIGURES

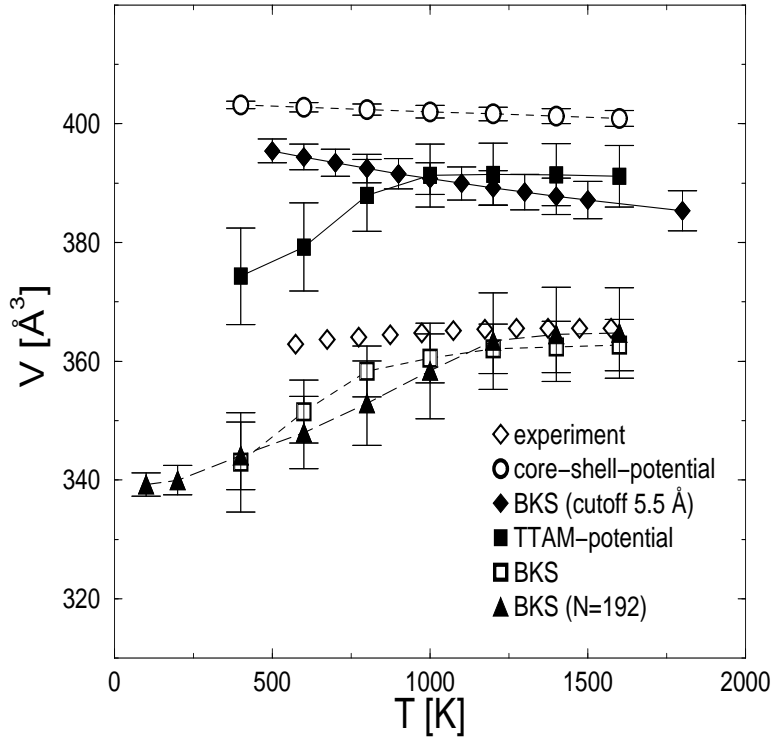


FIG. 1. Classical ( $P=1$ ) unit cell volume for  $\beta$ -cristobalite. The simulation box is a cube containing 27 unit cells with  $N = 648$  particles, except otherwise noted. Comparison with experimental data taken from Ref.<sup>10</sup>.



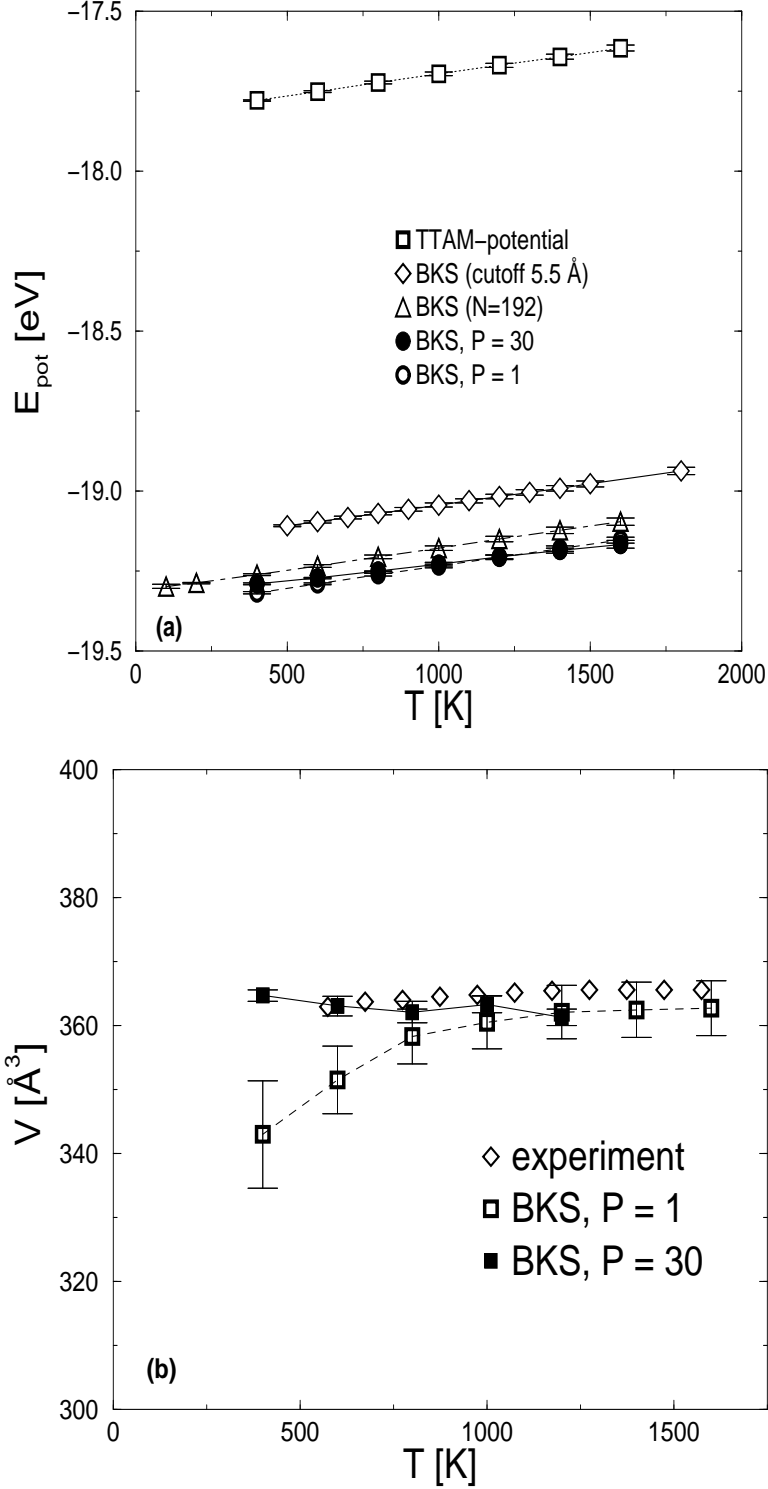


FIG. 2. Potential energy (a) and unit cell volume (b) for  $\beta$ -cristobalite, results of path integral Monte Carlo simulations (with  $N = 648$  particles and 27 unit cells unless otherwise noted). Comparison with experimental data taken from Ref.<sup>10</sup>. In addition simulations have been done with a “core-shell” potential<sup>6</sup> (see text) with an average potential energy of about -43.2 eV.

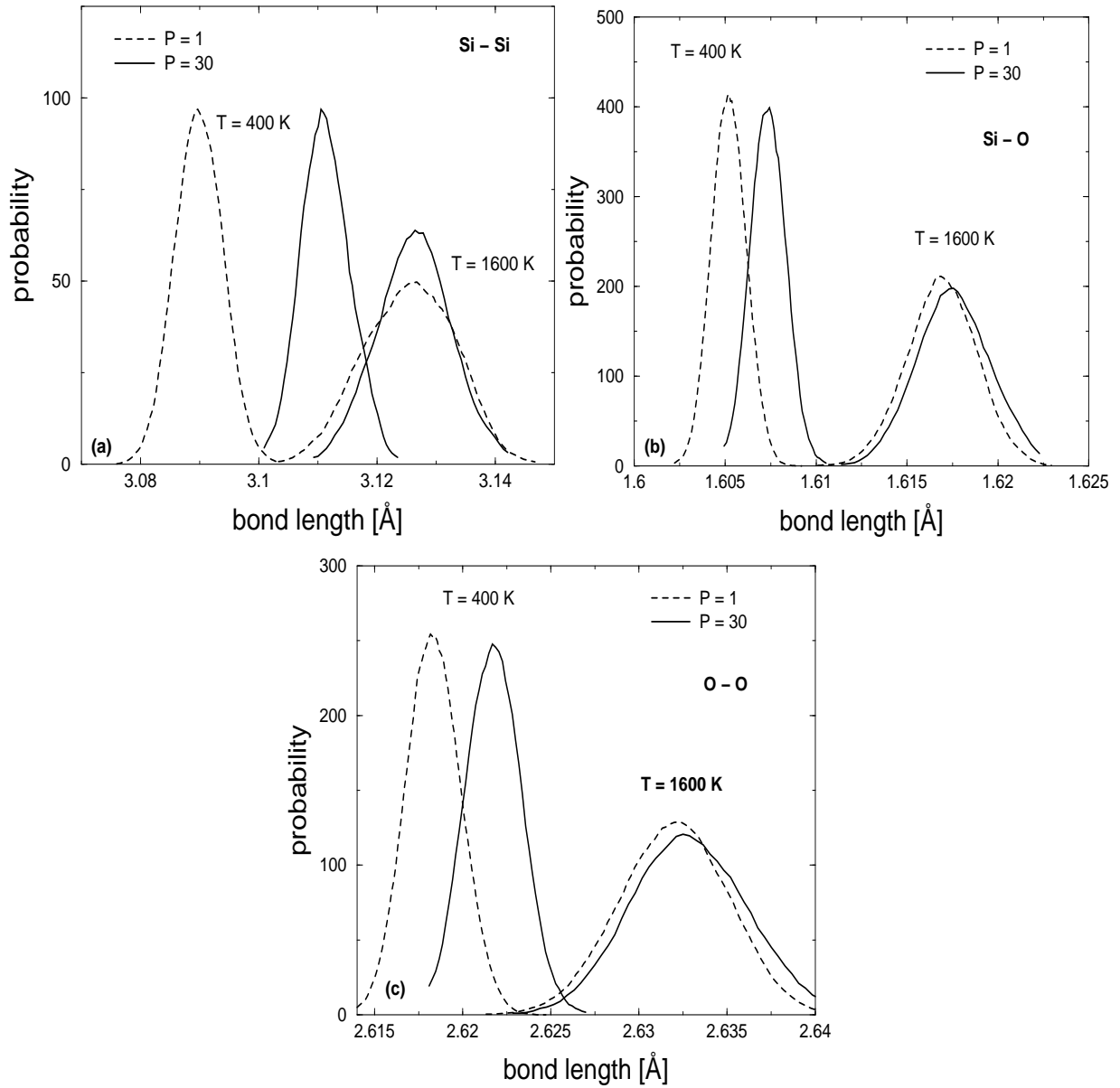


FIG. 3. Distributions of the bond lengths in  $\beta$ -cristobalite at the temperatures  $T = 400 \text{ K}$  and  $1600 \text{ K}$ . (a) Si-Si bonds, (b) Si-O bonds, (c) O-O bonds. Comparison of classical ( $P=1$ ) and quantum simulations ( $P=30$ ).

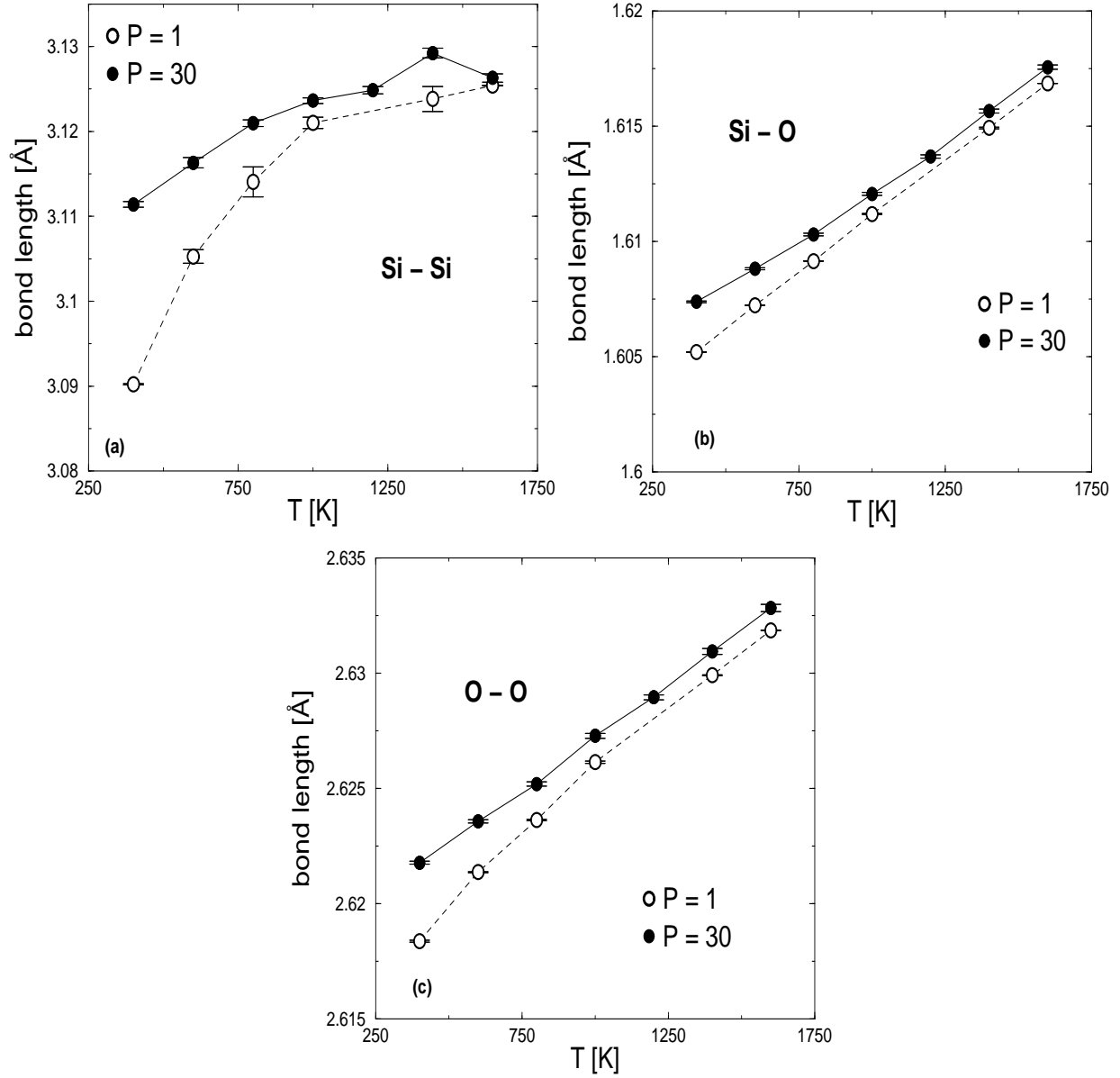


FIG. 4. Bond lengths between nearest neighbours in  $\beta$ - cristobalite. (a) Si-Si bonds, (b) Si-O bonds, (c) O-O bonds. Comparison of classical ( $P=1$ ) and quantum simulations ( $P=30$ ).

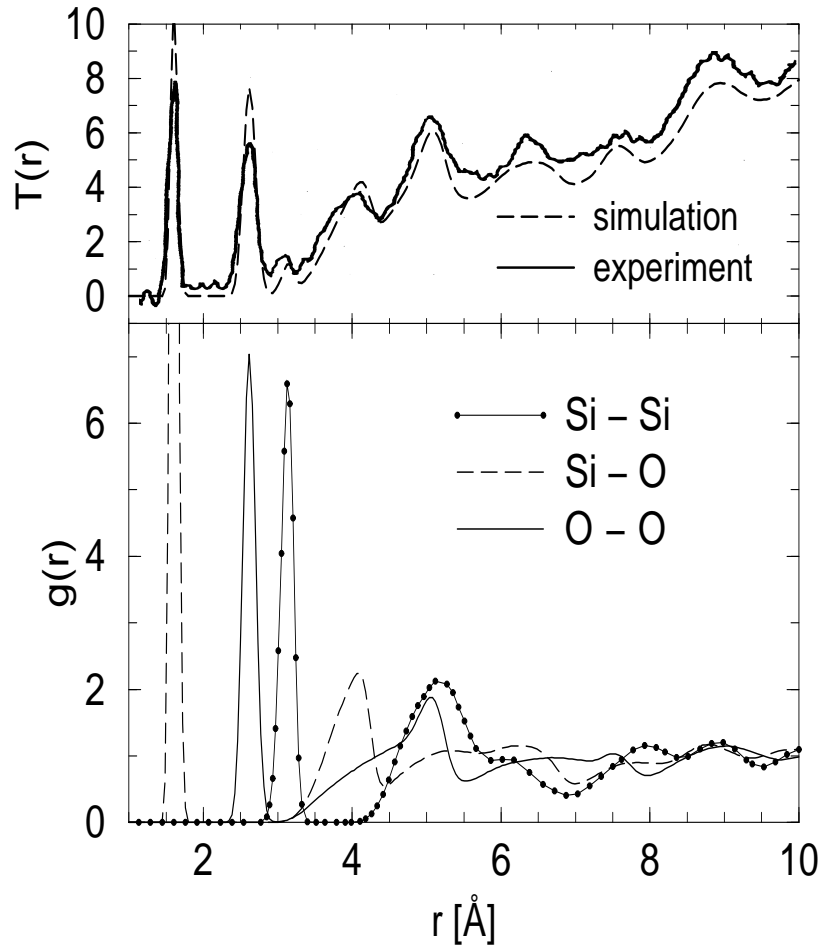


FIG. 5. a)  $T(r)$  for  $\beta$ -cristobalite as a function of distance  $r$  at 573 K. Experiment is represented by a solid line and simulation data is represented by a dashed line. b) Corresponding radial distribution function  $g(r)$  for Si-Si, Si-O, and O-O bonds. The curves are normalized such that  $g(r) \rightarrow 1$  for  $r \rightarrow \infty$ .

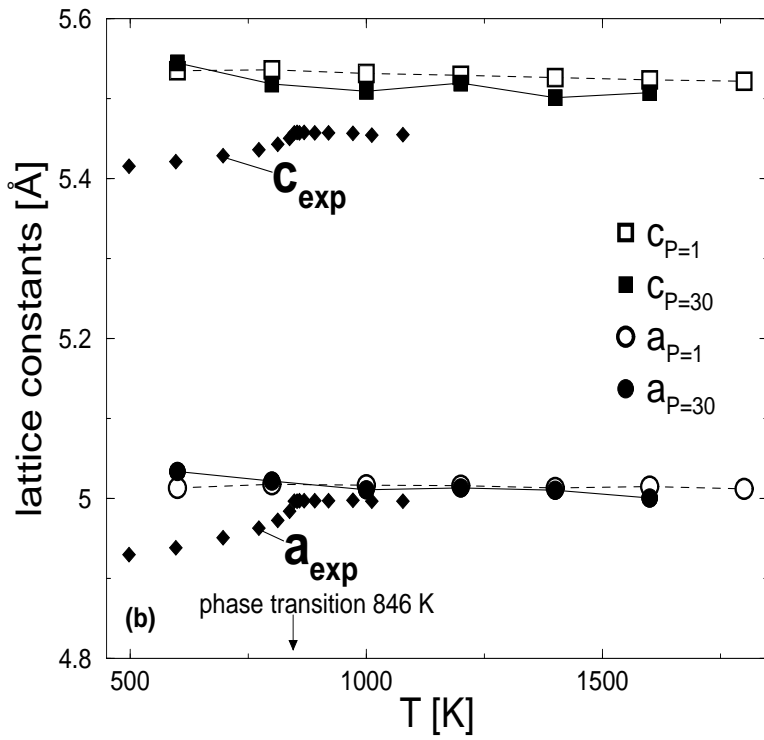
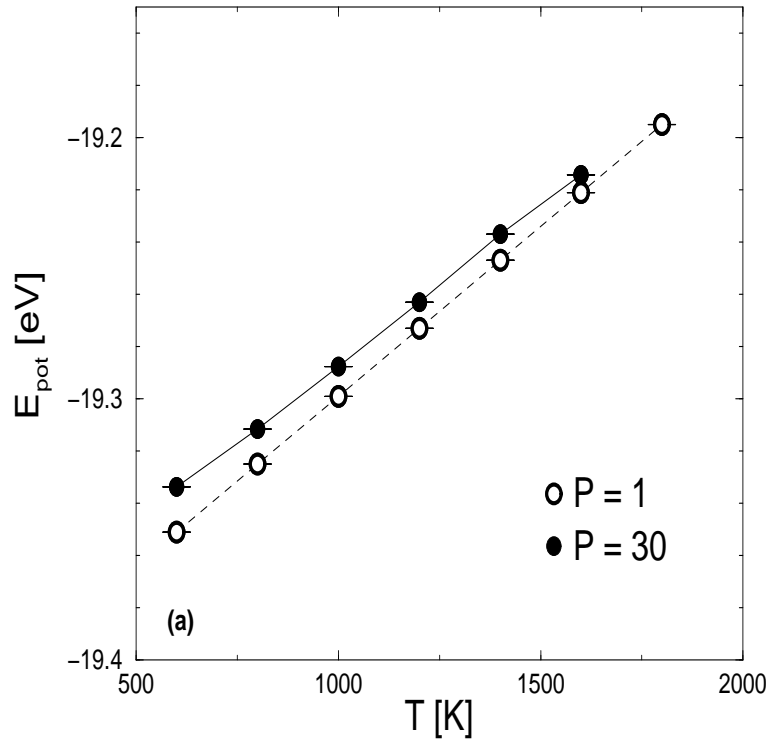


FIG. 6. Potential energy (a) and lattice constants (b) of  $\beta$ -quartz using the BKS potential

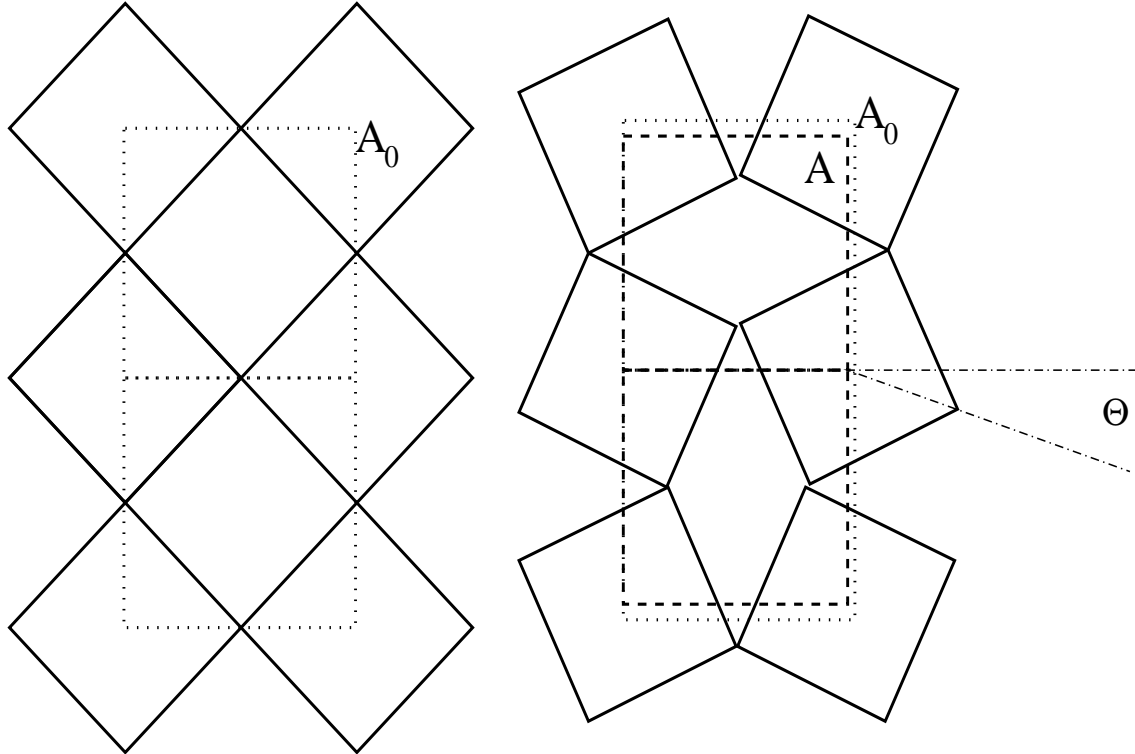


FIG. 7. Schematic picture of rigid unit modes in two spatial dimensions. By rotation of the unit cells (squares) by the angle  $\Theta$  the volume of the system can be reduced. Comparison of the system volume  $A_0$  with  $\Theta = 0$  (left side, dotted line) with the system volume  $A$  with  $\Theta \neq 0$  (right side, dashed line).

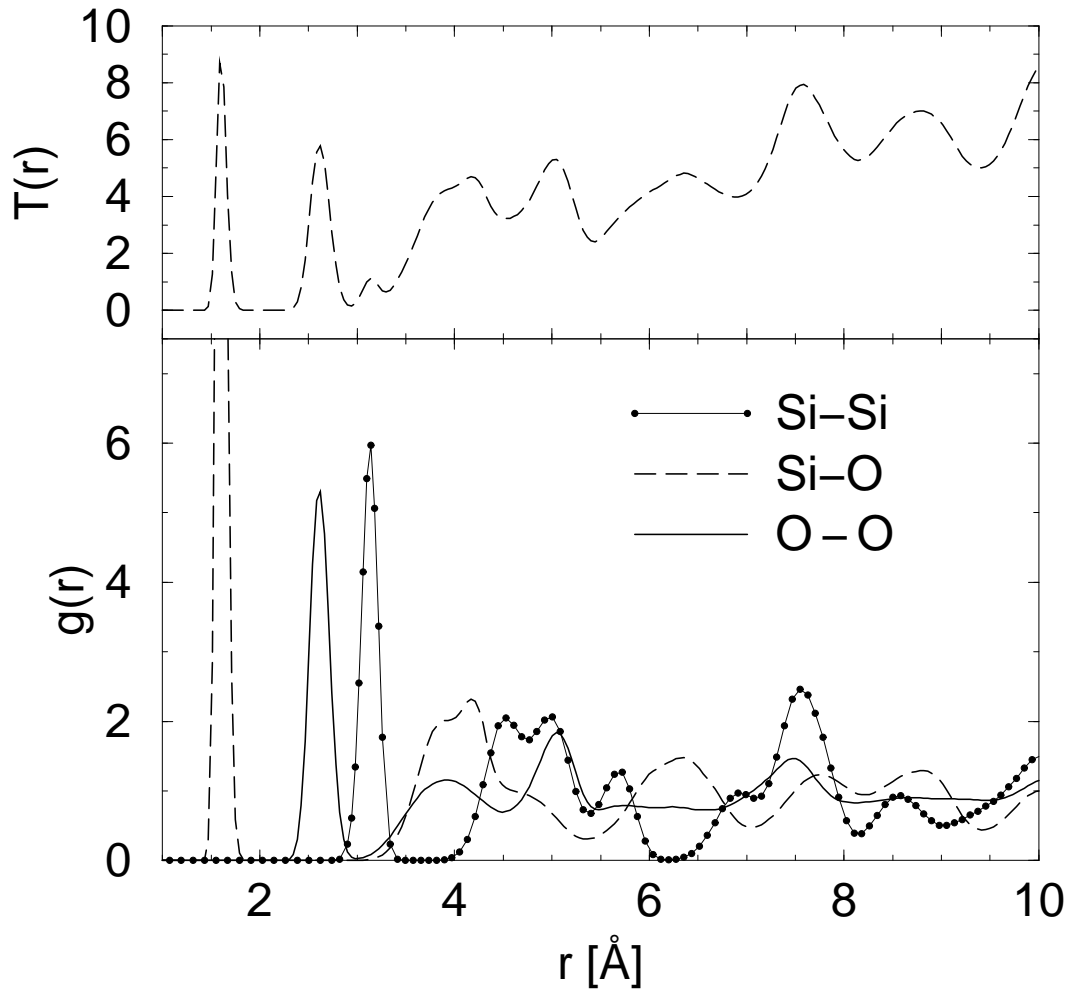


FIG. 8. a)  $T(r)$  for  $\beta$ -quartz as a function of distance  $r$  at 900 K. b) Corresponding radial distribution function  $g(r)$  for Si-Si, Si-O, and O-O bonds. The curves are normalized such that  $g(r) \rightarrow 1$  for  $r \rightarrow \infty$ .

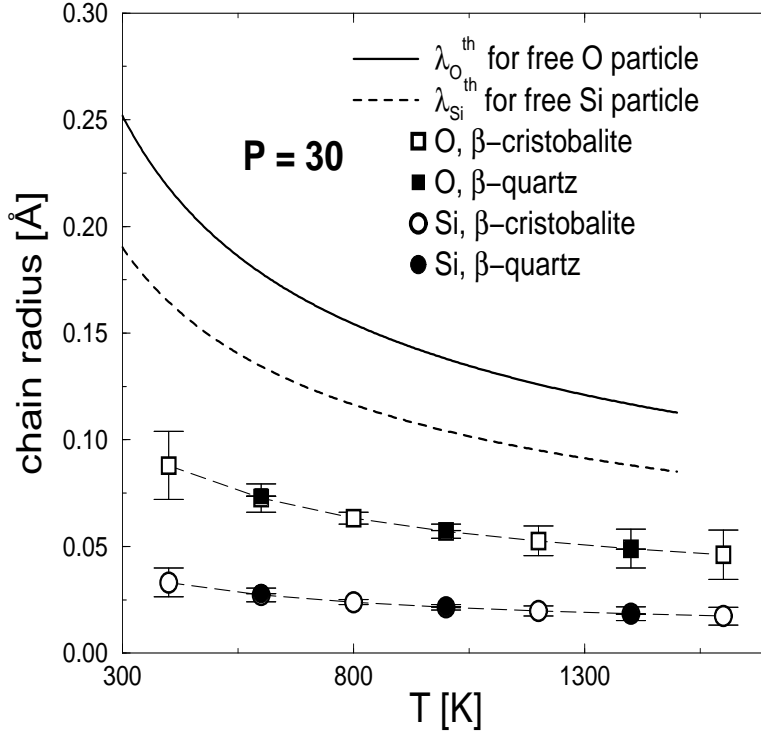


FIG. 9. Quantum chain radii in  $\beta$ - cristobalite and  $\beta$ - quartz. Comparison with the de- Broglie wave lengths of free particles



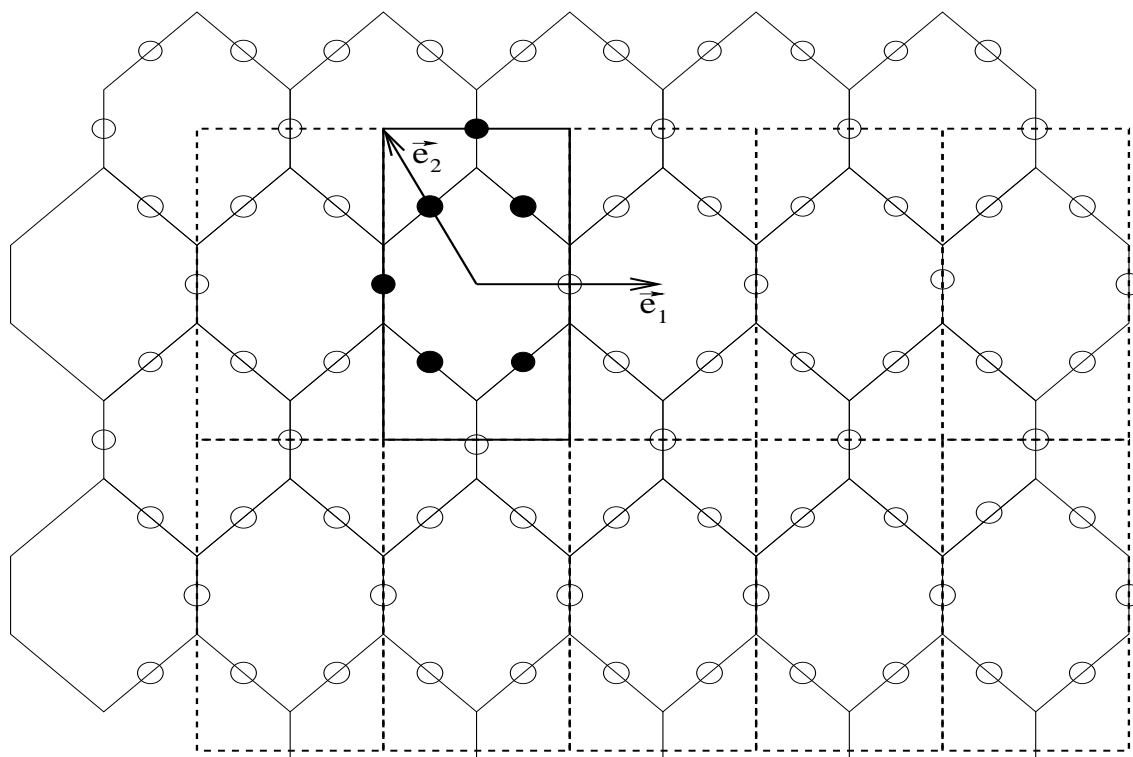


FIG. 10. Hexagonal unit cell of  $\beta$ -quartz, unit vectors, atom positions and orthogonal simulation box.

TABLES

ion pair	A/eV	B/Å <sup>-1</sup>	C/eVÅ <sup>6</sup>
Si-Si	872.4	15.22	23.265
O-O	1756.98	2.846	214.75
Si-O	10722.23	4.796	70.739

TABLE I. Parameters in Eq.(1) for the TTAM-potential.

ion pair	A/eV	B/Å <sup>-1</sup>	C/eVÅ <sup>6</sup>
Si-Si	0	-	0
O-O	1388.7730	2.76000	175.0000
Si-O	18003.7572	4.87318	133.5381

TABLE II. Parameters in Eq.(1) for the BKS-potential.

atom	x	y	z
Si 1	1/2	0	0
Si 2	0	1/2	2/3
Si 3	1/2	1/2	1/3
O 1	x	2x	1/2
O 2	$\bar{x}$	$\bar{2}x$	1/2
O 3	$\bar{2}x$	$\bar{x}$	1/6
O 4	x	$\bar{x}$	5/6
O 5	$\bar{x}$	x	5/6
O 6	2x	x	1/6

TABLE III. Coordinates of the particles in the unit cell of  $\beta$ -quartz (see Fig. 10).

atom	x/ $\text{\AA}$	y/ $\text{\AA}$	z/ $\text{\AA}$
Si 1	2.498850	0	0
Si 2	-1.249425	2.164068	3.640067
Si 3	1.249425	2.164068	1.820033
O 1	0	1.793579	2.730050
O 2	2.498850	2.534556	2.730050
O 3	0.945565	3.431346	0.910017
O 4	-0.945565	3.431346	4.550083
O 5	3.444415	0.896790	4.550083
O 6	1.553285	0.896790	0.910017

TABLE IV. Cartesian coordinates of the particles in the unit cell of  $\beta$ -quartz.